Low-loss, efficient, wide-angle 1×4 power splitter at ∼1.55 μm wavelengths for four play applications built with a monolithic photonic crystal slab

Jian Zhou,[1] Huiping Tian,[1,2,*] Daquan Yang,[1] Qi Liu,[1] Lijun Huang,[1] and Yuefeng Ji[1]

[1]The State Key Laboratory of Information Photonics and Optical Communications, School of Information and Communication Engineering, Beijing University of Posts and Telecommunications, Beijing 100876, China

[2]Beijing University of Posts and Telecommunications, P.O. BOX 90, No. 10 Xitucheng Road Haidian District, Beijing 100876, China

*Corresponding author: hptian@bupt.edu.cn

Received 8 July 2014; revised 17 October 2014; accepted 24 October 2014; posted 28 October 2014 (Doc. ID 216562); published 21 November 2014

We exhibit a low-loss, efficient, and wide-angle 1 × 4 power splitter based on a silicon monolithic photonic crystal slab with triangular lattice air holes. A distinctive power-splitting ratio can be obtained depending on the hole shift in the bending region and the structure adjustment at the junction area with regard to the power splitter designed. Simulation results achieved with a rigorous finite-difference time-domain technique show that the TE-polarized light is designed to ensure single-mode operation and the transmitted power is distributed almost equally, with a total transmission of 93.4% at the 1550 nm optical operation wavelength. Furthermore, we demonstrate ultralow-loss output of the optimized power splitter, with a transmittance above 22.5% (−6.48 dB) achieved in the ranges of 1524–1594 and 1610–1620 nm, which cover the entire C-band and a large portion of the L-band of optical communication.

OCIS codes: (130.3120) Integrated optics devices; (230.5298) Photonic crystals; (200.4650) Optical interconnects.

http://dx.doi.org/10.1364/AO.53.008012

1. Introduction

The efficient interconnection and guiding of light on a chip are crucial for telecommunication and optical computing applications [1]. Conventional dielectric waveguides support the guided mode along straight lines with high efficiency yet are restricted by radiation loss to the bending region. A recent theoretical investigation has been made that photonic crystal (PhC) holds the key for overcoming this difficulty. PhCs, also known as photonic bandgap (PBG) materials, are artificially engineered dielectric materials that exhibit a frequency regime over which the propagation of light is severely restricted [2,3]. A line defect in a PhC can give rise to a band of defect states within the gap and act as a waveguide. Well-designed PhC waveguides (PhCWs) can support good transmission through sharp-bend and Y-branch structures. They can be a promising candidate for the development of ultra-compact photonic integrated circuits (PICs) [4–6].

In recent years, PhC slab devices, based on triangular arrangements of low-index dielectric pillars in a high-index material, are much easier to fabricate and more reliable for practical applications. PhC devices fabricated by dielectric rods in air, in contrast, induce more out-of-plane losses due to the insufficiently vertical confinement by the total internal reflection (TIR). Some researchers have applied

1559-128X/14/348012-08$15.00/0

high-index segments in the dielectric rods leading to vertical confinement, resulting in extremely low out-of-plane losses in the PhC slab waveguides [7]. However, to some extent, this dielectric rod device adds to the fabrication complexity.

The PhC-slab-based beam splitter is indispensable in PICs, and a 1×2 beam splitter is the most fundamental element. To date, a large amount of components have been designed and fabricated using primary beam splitters (including by direct splitting), such as Y-branch [8,9] and T-branch [10,11] splitters, the directional coupling splitter [12,13], and the self-collimated beam splitter [14–17]. In addition, recently there has been growing interest in 1×3 PhC power splitters, enabling triple play capabilities. By applying the multimode interference technique [18], coupling [19,20], or the structure tuning method [21], researchers have demonstrated a 1×3 power splitter theoretically and experimentally. During the past few years, a large amount of properties of bend waveguides (such as single-bend waveguide, 1×2, 1×3) have been reported. Zhou *et al.* [22] demonstrated a single-bend waveguide that relied on displacing holes in the bending region, at the same time adjusting the size of the air holes to achieve low dispersion and a transmission spectrum present flatness over a 180 nm bandwidth around 1550 nm. Chen *et al.* [8] demonstrated a 1×2 power splitter based on the capsule-shaped design or the ARROW-B structure in which the bend loss was 1 dB/bend for a wavelength ranging from 1.50 to 1.58 μm, covering the C-band frequency. Beyond that, a 1×3 power splitter based on a silicon PhC slab with triangular lattice air holes was presented by Tee *et al.* [21] that showed the transmitted power was distributed almost equally, with a total normalized transmission of 99.74% and negligible reflection loss at the 1550 nm operating wavelength. However, in order to fulfill the higher integration requirement for compact optical integrated devices, we design a 1×4 power splitter on a monolithic PhC slab.

In this work, we present and model a 1×4 power splitter for which the discontinuities in the splitter and bending regions are carefully positioned, thereby ensuring ultralow-loss splitting for TE-polarized light within a broad band. With the finite-difference time-domain (FDTD) technique, we demonstrate that ultralow-loss transmission of each route (1, 2, 3, 4) above 22.5% (almost −6.48 dB) was obtained in the ranges of 1524–1594 and 1610–1620 nm, which cover the entire C-band and a large portion of the L-band of optical communication. In addition, the power is distributed almost equally, with a total normalized transmission of 93.4% and negligible reflection loss at the 1550 nm optical operating wavelength. More importantly, we mainly consider shifting the independent holes and slightly changing the radius of the holes surrounding the junctions. In the design in Ref. [23], Sakakura *et al.* demonstrated the fabrication of 1×4 splitter waveguides by creating four beam spots of femtosecond laser pulses inside a glass substrate with a spatial light modulator, which increased the fabrication complexity. The advantage is that the structure of the waveguide is continuous in the branching region of the 1×4 power splitter, while the waveguide was disconnected in the branching region in other work [24].

2. Design and Numerical Analysis

A basic air-bridge-type PhC-slab-based power splitter is formed by a triangular lattice of air cylinders etched in silicon with a refractive index of 3.4 ($n_{si} = 3.4$). The lattice pitch is $a = 425$ nm and the air hole diameter is $d = 2r = 0.64a = 272$ nm. It consists of three Y branches with a 120° angle. Generally, the waveguides are similar, and the light is incident and the output is measured from the position indicated in Fig. 1. The optimization of the Y branch, depicted by the orange dashed line and the shadow region, has been discussed by Yang *et al.* [9]. The radius of the green holes is $rx_2 = 0.32a = 136$ nm, and the shift is $\Delta_1 = 0.28a = 119$ nm in bend waveguide region no. 1. The red hole radius is $rx_1 = 0.20a = 85$ nm in the junction.

The modified power splitter is shown between straight waveguide region no. 2 and straight waveguide region no. 3 in Fig. 1, where the design has been changed at the junction area of the branches and the bending regions. The small holes (the yellow holes, with radius rx_4) at the center junctions are designed to interact with the incoming electromagnetic wave while they reduce the reflection loss and guide the wave into the branches effectively. The holes at the apex of the bending region are shifted along the symmetry axis of the bend, and they have been well studied by Zhou *et al.* [22]. Adding small holes at the junctions combined with shifting holes at the apex of bend, thus, eliminates the multimode effects [25] and gives rise to high transmittance. The main parameters of the optimized structure are rx_3, rx_4, rx_5, Δ_0, Δ_2, Δ_3, and Δ_4, where rx_3 is the radius of the hole at the apex of the upward bend, rx_4 and Δ_2 are the radius and the shift of the hole at the center junctions, respectively, rx_5 is the radius of the next hole at the center junctions, Δ_0 is the shift of the red hole (rx_1) in the shadow region in the opposite direction along the $\Gamma - K$ direction of the triangular lattice, and Δ_3 and Δ_4 are the shifts of the holes along the symmetric axis of the bending region in the same direction.

In our paper, the plane wave expansion (PWE) method and the open-source FDTD software Meep are used to calculate their photonic band structure and transmission spectra, respectively [26,27]. During the simulation, we set the incident light at the head of the entrance and monitor (1, 2, 3, 4) located at the end of the output based on the structure. Simultaneously, we use the TE-polarized Gaussian-pulse source (pulse light source centered at $\lambda =$ 1.55 um) as the incident source. The simulations are performed by using Meep to analyze the steady-state electric field (the TE-polarized continuous-pulse

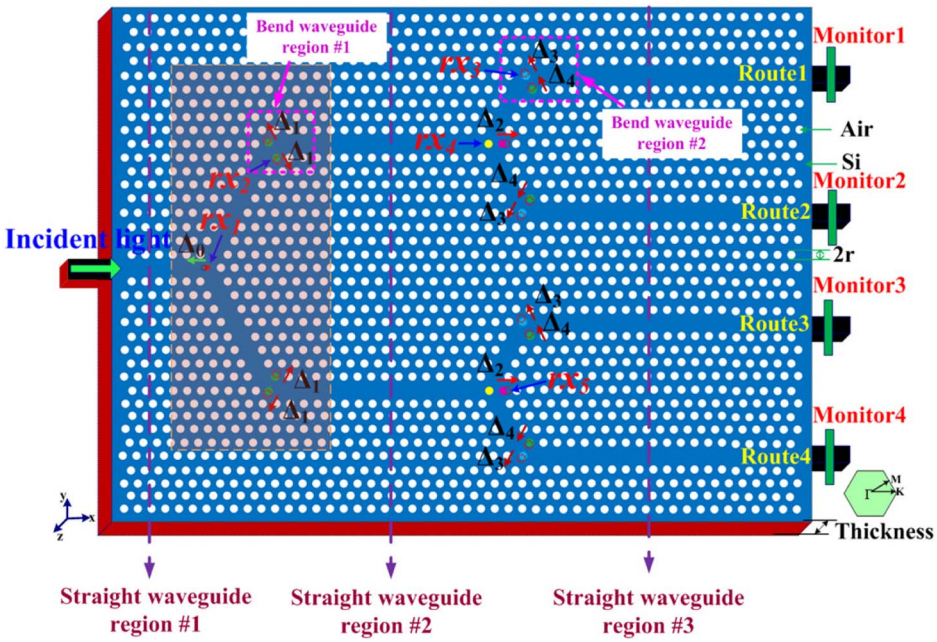

Fig. 1. Schematic view of the 2D PhC slab 1 × 4 power splitter, where $a = 425$ nm, $r = 0.32a$, rx_1 is the radius of the red holes at the center of the junction in the shadow region, rx_2 is the radius of the green holes at the bending regions, rx_3 is the radius of the light blue holes at the bending regions, rx_4 is the radius of the yellow holes at the center of the junctions between straight waveguide region nos. 2 and 3, rx_5 is the radius of the pink holes next to the yellow holes (rx_4), Δ_0 is the shift of the red hole (rx_1) in the opposite direction along the Γ – K direction of the triangular lattice, Δ_1 is the shift of the green holes (rx_2) in the opposite direction along the symmetric axis of the bend, Δ_2 is the shift of the pink holes (rx_5) along the Γ – K direction of the triangular lattice, and Δ_3 and Δ_4 are the shifts in the same direction along the symmetric axis of the bend.

source) and transmittance spectra. In order to improve accuracy in the process of simulation, FDTD analysis of the PhC structure is carried out with a mesh size of $a/20$, and to obtain a stable simulation, one must adhere to the Courant condition, which relates the spatial and temporal step size,

$$c\Delta t < \frac{1}{\sqrt{(1/\Delta x^2 + 1/\Delta y^2 + 1/\Delta z^2)}}, \qquad (1)$$

where c is the velocity of light, for the case of a nonuniform grid; the grid sizes represent the smallest grid size in the simulation. The temporal step size is chosen as $0.025a/c$ to satisfy the Courant condition and reduce the computation time at the same time. We have employed 10,000 iterations for the FDTD computation to obtain the steady-state results. All the simulations are carried out with the same mesh size and temporal step for future comparable results. The boundary conditions at the spatial edges of a finite computational region must be carefully considered. Therefore, a one-spatial-unit-thick perfectly matched layer is applied at the boundary regions to absorb the entire outward propagating electromagnetic wave without inducing reflections. The TE-polarized light has been used for the simulation, with its magnetic field only in the z direction (H_z) and the electric field in both x and y directions (E_x and E_y). The overall size of the splitter is about 22 μm × 14 μm, and it can be further reduced because the structure is only altered at the junction areas and bending regions. Such a small size makes it promising for future ultra-compact photonic integrated optical devices.

Our proposed PhC slab 1 × 4 power splitter is shown in Fig. 1. There are three straight waveguide sections: a single-mode input straight waveguide region no. 1, two single-mode transition straight waveguide regions no. 2, and four single-mode output straight waveguide regions no. 3 all along the Γ–K direction. We consider the process of propagation through the bend as follows [22]: light propagates along the straight waveguide in the Γ–K direction, then it couples with and turns into the mode in the Γ–M direction, and finally it couples back to the mode in the Γ–K direction again. Because the PBG and TIR prohibit light from scattering out of the structure, only reflection needs to be considered. Furthermore, the bend can be accurately described by a one-dimensional model determined only by the propagation constants (k) of the modes propagating in each direction [28]. Generally, one can achieve high transmission when the propagation constant in the Γ–K direction is matched with that in the Γ–M direction, because the light wave experiences the least difference between propagating along the straight waveguide and the bend waveguide. Only TE polarization is calculated in the simulation. The TE-like modes are even (symmetric) and odd (antisymmetric) about the mirror symmetry plane ($x = 0$).

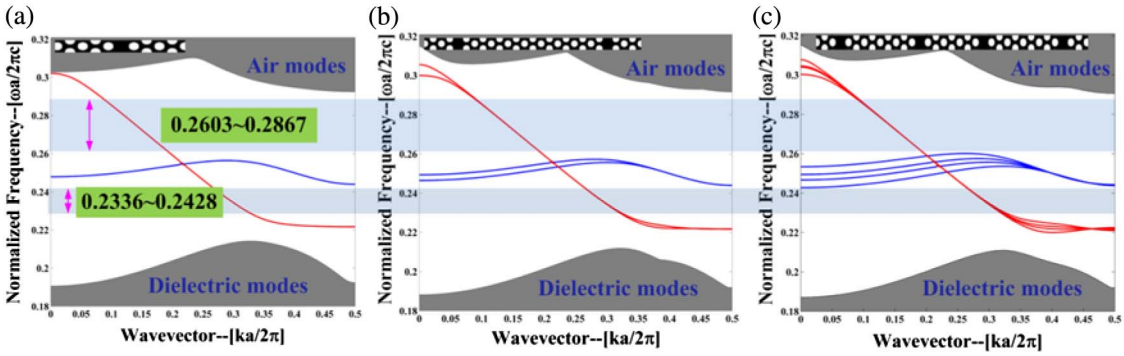

Fig. 2. Dispersion diagrams for TE polarization of three straight PhCW regions calculated using the plane wave expansion method. The supercells are shown in the insets. The red and blue lines represent even and odd gap-guided modes, respectively. The shadow region represents the span where high transmittance is obtained.

By the PWE method, the in-plane normalized dispersion diagrams for single-mode and multimode straight PhCWs are calculated and shown in Fig. 2. Supercells are depicted as insets. Single-mode W1 PhCW region no. 1 supports one even mode [Fig. 2(a)], and then multimode transition straight waveguide region no. 2 and output straight waveguide region no. 3 support two and four even modes [Figs. 2(b) and 2(c)], respectively. In order to realize high transmittance, the single-mode frequency span should be close to that of the multimode counterpart in the transition and output regions, and this means when the normalized frequency is (0.2603–0.2867)(a/λ) or (0.2336 – 0.2428)(a/λ), the light wave experiences the least difference in the process of propagation. Thus, high transmission is conceivable in this 1 × 4 power splitter based on the monolithic PhC slab design.

3. Results and Discussion

To evaluate the advantages of the proposed structure, the basic power splitter without optimization is simulated. The steady state of the z component of the magnetic field (H_z) is shown in Fig. 3. The low magnitude of the field is due to higher confinement and reflection near the bending regions. In addition, the discontinuity at the bend region stimulates higher-order modes that are evanescent in the PhCW. The measured powers are normalized with respect to the total power. The elemental splitter has high reflection loss at each route. The wide-angle splitting at the junction area leads to the incoming single-mode electromagnetic wave transforming into multimode. The single-mode routes experience mismatch with the incoming multimode electromagnetic wave, and thus, a considerable portion of power is lost and consequently the low measured powers are obtained. In the proposed design, adding and shifting holes are utilized to prevent the multimode propagation and mismatch from occurring. In addition, the hole radius can be altered to match the impedance of the waveguides, resulting in equal distribution of the incoming single-mode wave into four single-mode waves propagating in the routes.

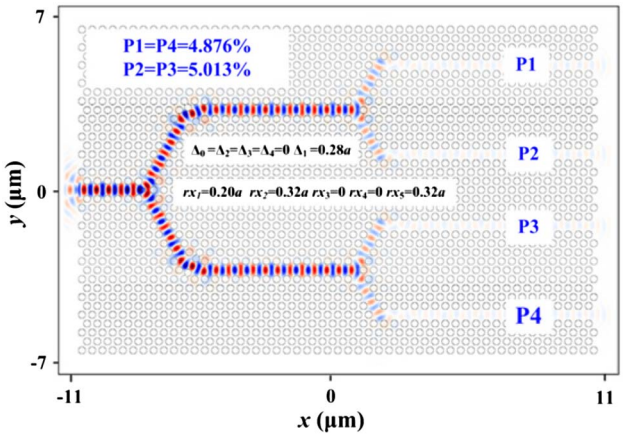

Fig. 3. Basic 1 × 4 power splitter design. Normalized output transmission powers are shown in the top left corner. The center inset is the parameter design of the structure.

Unlike the mode system of dielectric pillars in air [29], real optical systems consisting of air holes in dielectrics tend to be multimode. Multimode results in mode-mixing problems at intersections and difficulties in matching input and output fields at discontinuities, thus leading to high reflection loss. The transmission power through a junction relies strongly on the relationship between the modes that may propagate in the PhCW and the junction region [12]. To improve the transmission power, the wise choice is to modify the junction region. Through adding a smaller hole (the yellow holes, radius is rx_4) and moving the holes (the pink holes, radius is rx_5, with shift Δ_2) at the center of the junction region (Fig. 1), we change the size of the junction region, therefore eliminating multimode effects. The steady-state magnetic field (H_z) distribution at $rx_4 = 0.30a$ is shown in Fig. 4(a), indicating a slight improvement of transmission power. The normalized transmitted power at P1 and P4 is 7.876%, and at P2 and P3 it is 7.954%. The steady-state magnetic field (H_z) distribution at $rx_4 = 0.30a$, $\Delta_2 = 0.20a$, is shown in Fig. 4(b), indicating a slight improvement in transmission power compared with Fig. 4(a). The normalized transmitted power at P1 and P4 is 8.031%, and

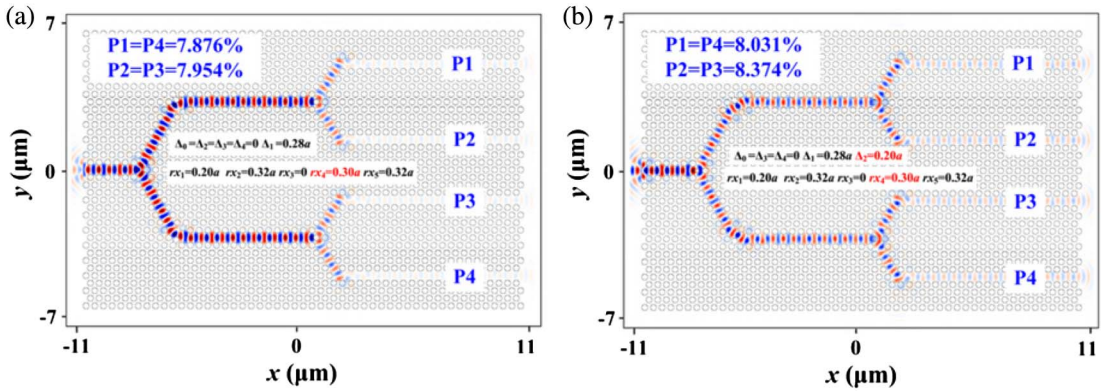

Fig. 4. Steady-state magnetic field (H_z) distribution at (a) $rx_4 = 0.30a$, (b) $rx_4 = 0.30a$, $\Delta_2 = 0.20a$, at 1550 nm wavelength. Normalized output transmission powers are shown in the top left corners. The center inset is the parameters design of the structure.

at P2 and P3 it is 8.374%. The slight improvement is mainly attributed to the reduced reflection loss of the bending regions.

Based on Fig. 4, we also find a sensitive analysis performed in [30], where the holes strongly influence the transmitted power at the apex of the bending region (the light blue holes and the green holes in Fig. 1). By adjusting the position and size of the holes at the apex of the bending corner, the wave number of the mode in the PhCW bend matches that of the PhC straight waveguide, as shown in Ref. [31]. We therefore restrict ourselves to a rigorous optimization of these four holes to limit computational cost. The proposal for symmetry and the restriction to only the two holes closest to the apex of the bend leave two optimized degrees of freedom: moving these two holes along the symmetry axis of the bend. The steady-state magnetic field (H_z) distribution at $rx_4 = 0.30a$, $\Delta_2 = 0.20a$, $rx_3 = 0.32a$, and $\Delta_3 = 0.36a$ is shown in Fig. 5(a), indicating a large improvement in transmission power compared with Fig. 4. The normalized transmitted power at P1 and P4 is 18.96%, and at P2 and P3 it is 17.6%. The steady-state magnetic field (H_z) distribution at $rx_4 = 0.30a$, $\Delta_2 = 0.20a$, $rx_3 = 0.32a$, $\Delta_3 = 0.36a$, and $\Delta_4 = 0.10a$ is shown in Fig. 5(b), indicating a slight optimization of transmission power. The normalized transmitted power at P1 and P4 is 19.85%, and at P2 and P3 it is 17.23%. Such great improvement at P1 and P4, mainly due to suppressed multimode behavior, shows a good impedance match between the straight waveguide and bend waveguide, and leads to a considerable reduction in reflection and dispersion loss. However, the power at P2 and P3 shows a slight decrease, resulting from the additional reflection loss.

In order to further improve the transmitted power and split the power equally into the output routes, we try to alter the position of the hole (the red hole; radius is rx_1, shift is Δ_0) at the center of junction in the shadow region. The routes' impendence should be similar and matched with the input straight waveguide [25]. The steady-state magnetic field (H_z) distribution at $rx_4 = 0.30a$, $\Delta_2 = 0.20a$, $rx_3 = 0.32a$, $\Delta_3 = 0.36a$, and $\Delta_0 = 0.06a$ in Fig. 6 shows a large improvement in transmission power compared to Fig. 5. The normalized transmitted power at P1 and P4 is 23.18%, and at P2 and P3 it is 23.52%. The total power arrives at 93.4%, suggesting a region of optimum operation as highlighted in Fig. 6. When we vary and shift the holes, different transmittance is achieved accordingly. Due to the nature of PBGs,

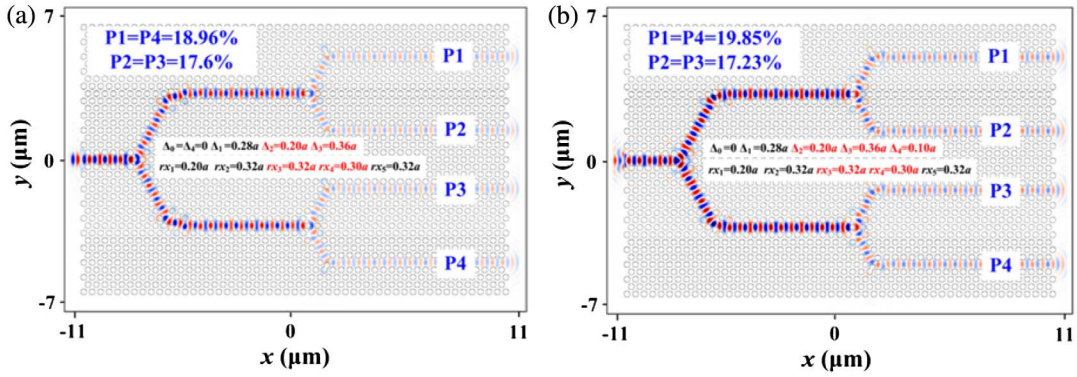

Fig. 5. Steady-state magnetic field (H_z) distribution at (a) $rx_4 = 0.30a$, $\Delta_2 = 0.20a$, $rx_3 = 0.32a$, $\Delta_3 = 0.36a$; (b) $rx_4 = 0.30a$, $\Delta_2 = 0.20a$, $rx_3 = 0.32a$, $\Delta_3 = 0.36a$, $\Delta_4 = 0.10a$ at 1550 nm wavelength. Normalized output transmission powers are shown in the top left corners. The center inset is the parameter design of the structure.

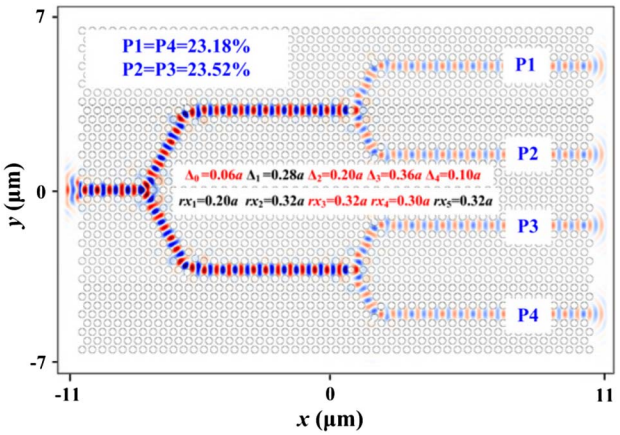

Fig. 6. Steady-state magnetic field (H_z) distribution at $rx_4 = 0.30a$, $\Delta_2 = 0.20a$, $rx_3 = 0.32a$, $\Delta_3 = 0.36a$, $\Delta_4 = 0.10a$, $\Delta_0 = 0.06a$, at 1550 nm wavelength. Normalized output transmission powers are shown in the top left corner. The center inset is the parameter design of the structure.

unlike conventional waveguides, PhCWs do not experience radiation loss. As depicted in [28], the reflection coefficient of the waveguide bend can be expressed as

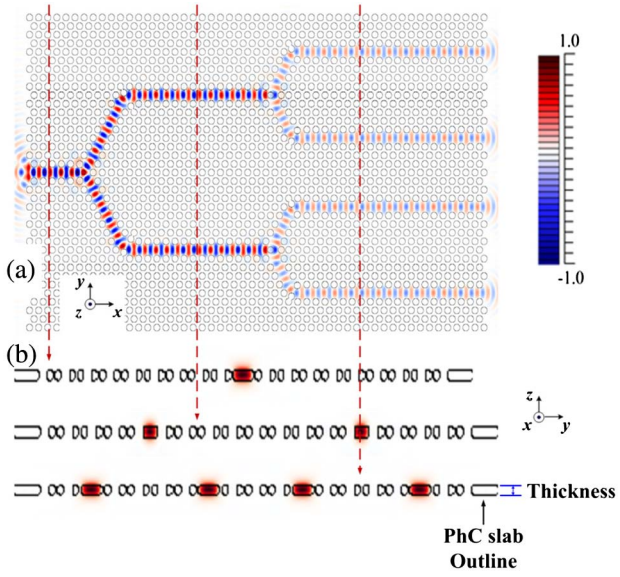

Fig. 7. Steady-state magnetic field (H_z) distribution for the fundamental TE-like mode propagating through the optimized PhC slab splitter in (a) the x–y plane and (b) the y–z plane [three transversal surfaces at the dashed lines in (a)].

$$R(\omega) = \left[1 + \left(\frac{2k_{\Gamma K}(\omega)k_{\Gamma M}(\omega)}{(k_{\Gamma K}^2(\omega) - k_{\Gamma M}^2(\omega))\sin(k_{\Gamma M}(\omega)L)}\right)^2\right]^{-1}, \tag{2}$$

where $k_{\Gamma K}$ and $k_{\Gamma M}$ are the wavenumbers of the modes in the straight waveguide and the waveguide bend, respectively, and L is the equivalent length of the bend. For the conventional triangular-lattice W1 waveguide in the Brillouin zone, the band diagram repeats with a period of $0.5(2\pi/a)$, and the corresponding $k_{\Gamma K}$ remains constant. When we vary and shift the holes, the relevant $k_{\Gamma M}$ and $\Delta k = |k_{\Gamma K} - k_{\Gamma M}|$ change. Thus, the $R(\omega)$ is varied from the expression and a different value of transmittance is obtained accordingly. Therefore, by optimizing the position and size of the holes, the reflection loss is largely reduced and an efficient transmission is achieved. Meanwhile, within the region, the normalized power transmission is nearly 23.35% for four output routes. Figure 7 shows the steady-state magnetic field (H_z) profile for the fundamental TE-like mode propagating through the optimum 1×4 power splitter based on a monolithic PhC slab when a Gaussian cw is excited from a light source with a center frequency $\omega_0 = 0.274(2\pi c/a)$. As seen in Fig. 7, the optical field is confined horizontally by a PBG provided by the PhC [Fig. 7(a)] and vertically by the TIR due to the refractive index difference between alternating layers [Fig. 7(b)]. Figure 8 shows the transverse profile of the magnetic field H_z of the supercells calculated by the PWE method in these regions: straight waveguide region no. 1, bend waveguide region no. 1, and bend waveguide region no. 2, respectively. Based on this optimum power splitter, the mode patterns appear similar in three regions simultaneously, and they are three even modes polarized along the propagation direction. Thus, although the existence of the bend waveguide makes the region not a single-mode operation, through design, step by step, the light from the straight waveguide will mostly couple with the mode in the bend waveguide with a matched mode pattern. Obviously, a highly efficient 1×4 power splitter is obtained.

In order to further demonstrate the performance of the optimum 1×4 power splitter in the range of the PBG, we calculate the transmission spectra of four routes (1, 2, 3, 4), as shown in Fig. 9. The thick black-dashed line represents the transmitted power

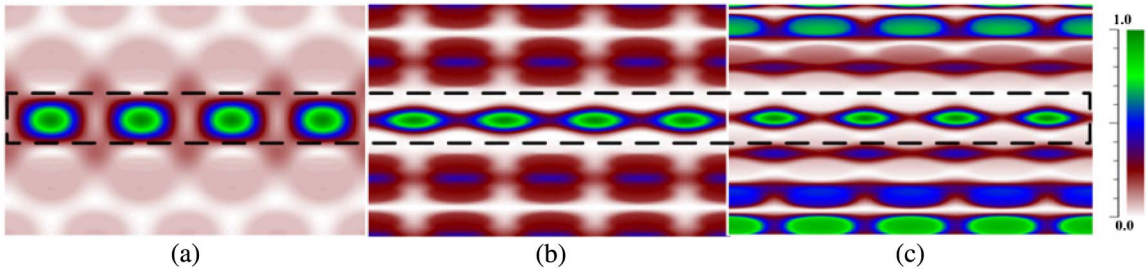

Fig. 8. Transverse profile of the magnetic field H_z in three regions: (a) straight waveguide region no. 1, (b) bend waveguide region no. 1, and (c) bend waveguide region no. 2.

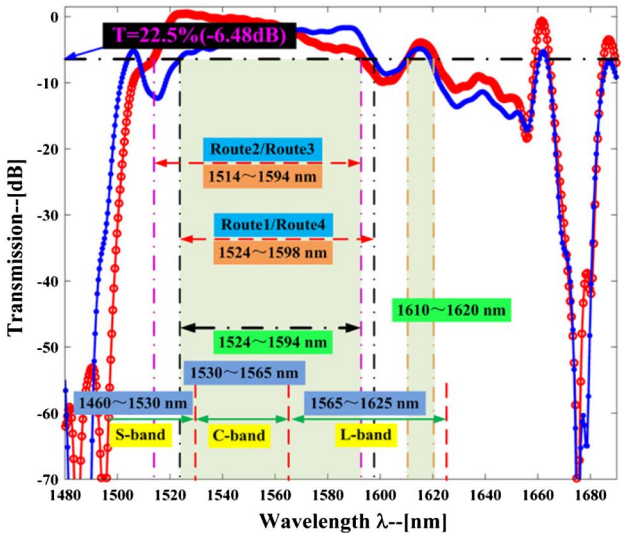

Fig. 9. FDTD transmission spectra (red and blue curves) for TE-polarized light at routes 2 and 3 and routes 1 and 4 at the output of the optimum 1 × 4 power splitter. The horizontal black dash-dotted line represents the transmission of 22.5% (–6.48 dB). Ultralow-loss output of the optimized power splitter with a transmission above 22.5% (–6.48 dB) is obtained in the ranges 1514–1594 and 1610–1620 nm for routes 2 and 3 and in the ranges 1524–1598 and 1610–1620 nm for routes 1 and 4; the structure covers the entire C-band and a large portion of the L-band of optical communication.

of 22.5% (–6.48 dB). An ultralow-loss output of the optimized power splitter with transmission above 22.5% (–6.48 dB) is obtained in the ranges of 1514–1594 and 1610–1620 nm for routes 2 and 3, and in the ranges of 1524–1598 and 1610–1620 nm for routes 1 and 4. Thus, the structure contains the ranges of 1524–1594 and 1610–1620 nm, which cover the entire C-band and a large portion of L-band of optical communication. The optimum 1 × 4 power splitter created based on the PBG principle can support single-mode behavior over a wide range of wavelengths. In the proposed splitter, similar transmitted power has been realized for the 1524–1594 and 1610–1620 nm wavelength ranges, opening up the potential for four play applications.

4. Conclusion

In this work, a 1 × 4 power splitter is proposed by shifting the holes in the bending region and modifying the region at the junction area. Through rigorous analysis, the power splitter is capable of dividing the electromagnetic wave total power desirably, where each route (1, 2, 3, 4) presents transmission of almost 23.35% at an operating wavelength of 1550 nm. In addition, ultralow-loss output of the optimized power splitter with a transmittance above 22.5% (–6.48 dB) is achieved in the ranges of 1524–1594 and 1610–1620 nm, which cover the entire C-band and a large portion of the L-band of optical communication. Compared with the optimization method demonstrated in Ref. [21], the fabrication complexity of this optimized scheme of a power splitter is lower. Therefore, this optimized 1 × 4 power splitter has more potential for realization of ultracompact, low-loss optical integrated circuits.

This research was supported by NSFC (No. 61372038), National 973 Program (No. 2012CB315705), National 863 Program (No. 2011AA010306), Postgraduate Innovation Fund of SICE, BUPT, 2013, and Fund of State Key Laboratory of Information Photonics and Optical Communications (Beijing University of Posts and Telecommunications), China.

References

1. Y. Zhang and B. Li, "Photonic crystal-based bending waveguides for optical interconnections," Opt. Express **14**, 5723–5732 (2006).
2. E. Yablonovitch, "Inhibited spontaneous emission in solid-state physics and electronics," Phys. Rev. Lett. **58**, 2059–2062 (1987).
3. S. John, "Strong localization of photons in certain disordered dielectric superlattices," Phys. Rev. Lett. **58**, 2486–2489 (1987).
4. M. Notomi, K. Yamada, A. Shinya, J. Takahashi, C. Takahashi, and I. Yokohama, "Extremely large group-velocity dispersion of line-defect waveguides in photonic crystal slabs," Phys. Rev. Lett. **87**, 253902 (2001).
5. S. H. G. Teo, A. Q. Liu, J. B. Zhang, M. H. Hong, J. Singh, M. B. Yu, N. Singh, and G. Q. Lo, "Photonic bandgap crystal resonator enhanced laser controlled modulations of optical interconnects for photonic integrated circuits," Opt. Express **16**, 7842–7848 (2008).
6. S. Matsuo, K. Takeda, T. Sato, M. Notomi, A. Shinya, K. Nozaki, H. Taniyama, K. Hasebe, and T. Kakitsuka, "Room-temperature continuous-wave operation of lateral current injection wavelength-scale embedded active-region photonic-crystal laser," Opt. Express **20**, 3773–3780 (2012).
7. A. A. M. Kok, J. J. G. M. van der Tol, R. Baets, and M. K. Smit, "Reduction of propagation loss in pillar-based photonic crystal waveguides," J. Lightwave Technol. **27**, 3904–3911 (2009).
8. J. H. Chen, Y. T. Huang, Y. L. Yang, and M. F. Lu, "Design, fabrication, and characterization of Si-based ARROW-B photonic crystal sharp-bend waveguides and power splitters," J. Lightwave Technol. **30**, 2345–2351 (2012).
9. D. Yang, H. Tian, and Y. Ji, "High-bandwidth and low-loss photonic crystal power-splitter with parallel output based on the integration of Y-junction and waveguide bends," Opt. Commun. **285**, 3752–3757 (2012).
10. J. S. Jensen and O. Sigmund, "Topology optimization of photonic crystal structures: a high-bandwidth low-loss T-junction waveguide," J. Opt. Soc. Am. B **22**, 1191–1196 (2005).
11. S. H. Fan, S. G. Johnson, J. D. Joannopoulos, C. Manolatou, and H. A. Haus, "Loss-induced on/off switching in a channel add/drop filter," Phys. Rev. B **64**, 245302 (2001).
12. W. Zheng, M. Xing, G. Ren, S. G. Johnson, W. Zhou, W. Chen, and L. Chen, "Integration of a photonic crystal polarization beam splitter and waveguide bend," Opt. Express **17**, 8657–8668 (2009).
13. M. Thorhauge, L. H. Frandsen, and P. I. Borel, "Efficient photonic crystal directional couplers," Opt. Lett. **28**, 1525–1527 (2003).
14. J. M. Park, S. G. Lee, H. R. Park, and M. H. Lee, "High-efficiency polarization beam splitter based on a self-collimating photonic crystal," J. Opt. Soc. Am. B **27**, 2247–2254 (2010).
15. Y. Xu, S. Wang, S. Lan, X. Lin, Q. Guo, and L. Wu, "Self-collimating polarization beam splitter based on photonic crystal Mach–Zehnder interferometer," J. Opt. Soc. Am. B **27**, 1359–1363 (2010).
16. V. Zabelin, L. A. Dunbar, N. L. Thomas, and R. Houdré, "Self-collimating photonic crystal polarization beam splitter," Opt. Lett. **32**, 530–532 (2007).

17. D. M. Pustai, S. Shi, C. Chen, A. Sharkawy, and D. W. Prather, "Analysis of splitters for self-collimated beams in planar photonic crystals," Opt. Express **12**, 1823–1831 (2004).
18. M. Zhang, R. Malureanu, A. C. Krüger, and M. Kristensen, "1×3 beam splitter for TE polarization based on self-imaging phenomena in photonic crystal waveguides," Opt. Express **18**, 14944–14949 (2010).
19. C. Y. Liu, "Fabrication and optical characteristics of silicon-based two dimensional wavelength division multiplexing splitter with photonic crystal directional waveguide couplers," Phys. Lett. A **375**, 2754–2758 (2011).
20. M. Djavid, A. Ghaffari, F. Monifi, and M. S. Abrishamian, "Photonic crystal power dividers using L-shaped bend based on ring resonators," J. Opt. Soc. Am. B **25**, 1231–1235 (2008).
21. D. C. Tee, T. Kambayashi, S. R. Sandoghchi, N. Tamchek, and F. R. M. Adikan, "Efficient, wide angle, structure tuned 1×3 photonic crystal power splitter at 1550 nm for triple play applications," J. Lightwave Technol. **30**, 2818–2823 (2012).
22. J. Zhou, H. Tian, D. Yang, Y. Liu, Q. Liu, and Y. Ji, "Ultra-broadband and ultra-low-loss photonic crystal with band-flatness waveguide 60° bend obtained based on lattice-shifted optimization," Opt. Commun. **322**, 227–233 (2014).
23. M. Sakakura, T. Sawano, Y. Shimotsuma, K. Miura, and K. Hirao, "Fabrication of three-dimensional 1×4 splitter waveguides inside a glass substrate with spatially phase modulated laser beam," Opt. Express **18**, 12136–12143 (2010).
24. M. Pospiech, M. Emons, B. Väckenstedt, G. Palmer, and U. Morgner, "Single-sweep laser writing of 3D-waveguide devices," Opt. Express **18**, 6994–7001 (2010).
25. S. Boscolo, M. Midrio, and T. F. Krauss, "Y junctions in photonic crystal channel waveguides: high transmission and impedance matching," Opt. Lett. **27**, 1001–1003 (2002).
26. J. D. Joannopoulos, S. G. Johnson, J. N. Winn, and R. D. Meade, *Photonic Crystals: Molding the Flow of Light*, 2nd ed. (Princeton University, 2008).
27. A. F. Oskooi, D. Roundy, M. Ibanescu, P. Bermel, J. D. Joannopoulos, and S. G. Johnson, "Meep: a flexible free software package for electromagnetic simulations by the FDTD method," Comput. Phys. Commun. **181**, 687–702 (2010).
28. A. Mekis, J. C. Chen, I. Kurland, S. Fan, P. R. Villeneuve, and J. D. Joannopoulos, "High transmission through sharp bends in photonic crystal waveguides," Phys. Rev. Lett. **77**, 3787–3790 (1996).
29. J. D. Joannopoulos, P. R. Villeneuve, and S. Fan, "Photonic crystals: putting a new twist on light," Nature **386**, 143–149 (1997).
30. K. Rauscher, "Simulation, design, and characterization of photonic crystal devices in a low vertical index contrast regime," Doctoral dissertation ETH 16516 (ETH Zurich, 2006).
31. G. Ren, W. H. Zheng, Y. J. Zhang, K. Wang, X. Y. Du, M. X. Xing, and L. H. Chen, "Mode analysis and design of a low-loss photonic crystal 60° waveguide bend," J. Lightwave Technol. **26**, 2215–2218 (2008).